

VLTI/MIDI 10 MICRON INTERFEROMETRY OF THE FORMING MASSIVE STAR W33A

W.J. DE WIT¹, M.G. HOARE¹, R.D. OUDMAIJER¹, J.C. MOTTRAM¹

Draft version August 16, 2021

ABSTRACT

We report on resolved interferometric observations with VLTI/MIDI of the massive young stellar object (MYSO) W33A. The MIDI observations deliver spectrally dispersed visibilities with values between 0.03 and 0.06, for a baseline of 45m over the wavelength range 8-13 μ m. The visibilities indicate that W33A has a FWHM size of approximately 120 AU (0.030 $''$) at 8 μ m which increases to 240 AU at 13 μ m, scales previously unexplored among MYSOs. This observed trend is consistent with the temperature falling off with distance. 1D dust radiative transfer models are simultaneously fit to the visibility spectrum, the strong silicate feature and the shape of the mid infrared spectral energy distribution (SED). For any powerlaw density distribution, we find that the sizes (as implied by the visibilities) and the stellar luminosity are incompatible. A reduction to a third of W33A's previously adopted luminosity is required to match the visibilities; such a reduction is consistent with new high resolution 70 μ m data from Spitzer's MIPS GAL survey. We obtain best fits for models with shallow dust density distributions of $r^{-0.5}$ and $r^{-1.0}$ and for increased optical depth in the silicate feature produced by decreasing the ISM ratio of graphite to silicates and using optical grain properties by Ossenkopf et al. (1992).

Subject headings: stars: formation — stars: early type — techniques: interferometric

1. INTRODUCTION

Massive young stellar objects are luminous, embedded infrared (IR) sources that show many signs that they are still actively accreting mass. Their luminosity ($L > 10^4 L_{\odot}$) is such that they are expected to be ionizing their surroundings to produce an H II region, yet they only have weak radio emission due to ionized winds or jets (Hoare 2002). Most appear to be driving bipolar molecular flows and (sub-)millimetre interferometry is beginning to reveal evidence of rotating, disc-like structures on scales of hundreds of AU (Patel et al. 2005; Beltrán et al. 2006; Torrelles et al. 2007). There is great interest in knowing the distribution of the infalling and outflowing material on smaller scales to provide clues to which physical processes are controlling the dynamics and setting the final mass of the star (Beuther et al. 2007; Hoare et al. 2007).

The mid-IR (8-13 μ m) emission from MYSOs is thought to arise in the warm (~ 300 K) dust in the envelope heated by the young star. Previous modelling (e.g. Churchwell et al. 1990) has indicated that the size of the mid-IR emission region should be unresolved at the typical distances of MYSOs by single-dishes and this is borne out by observations (Kraemer et al. 2001; Mottram et al. 2007). Exceptions occur when MYSOs are viewed close to edge-on when a dense torus can completely obscure the bright central region and only the warm dust in the outflow cavities is seen (de Buizer 2006).

Here we present new results from mid-IR interferometric observations of the MYSO W33A using the VLTI MIDI instrument. W33A has a kinematic distance of 3.8 kpc and a luminosity as derived from IRAS fluxes of $1 \times 10^5 L_{\odot}$ (Faúndez et al. 2004). It has weak, compact, optically thick radio continuum emission (Rengara-

jan & Ho 1996; van der Tak & Menten 2005) and broad (~ 100 km s $^{-1}$), single-peaked H I recombination emission lines (Bunn et al. 1995) consistent with an ionized stellar wind origin. IR images from 2MASS and Spitzer's GLIMPSE survey clearly show a large scale monopolar nebula emerging to the SE, which is most likely to demarcate the blue-shifted lobe of a bipolar outflow.

The cold dust envelope has been studied at a few arc-second resolution at millimetre wavelengths (van der Tak et al. 2000), probing the imprint of the star formation process on the circumstellar dust distribution. Many different scenarios have been put forward predicting this distribution. In case of W33A, Gürtler et al. (1991) modelled the SED with a constant density spherical envelope and found an inner cavity radius of 135 AU (35 mas at 3.8 kpc) with the dust close to the sublimation temperature. MIDI provides data on comparable size scales of 50 mas, and since the mid-IR size will be somewhat larger than the sublimation zone we expect the emission to be well-resolved.

2. OBSERVATIONS AND DATA REDUCTION

MIDI is the VLTI's two telescope beam combiner that operates in the thermal IR (Leinert et al. 2003). W33A was observed with MIDI on 16 September 2005, employing the UT2-UT3 telescope configuration for a projected baseline of 45.5 m and position angle of 47 $^{\circ}$ east of north; this is perpendicular to the star's outflow direction. An interferometric calibrator star HD 169916 was observed during the same night. Lunar occultation and indirect methods reveal the calibrator diameter to be a few mas (Nather 1972; Pasinetti-Fracassini 2001), too small to be resolved by MIDI. Here we present visibilities between 8-13 μ m that are spectrally dispersed at a resolution of $R = 30$. The observations were executed in the *High-Sens* MIDI mode (for details see Przygodda et al. 2003; Chesneau et al. 2005; Leinert et al. 2004). We summarize the main elements of the procedure that produces the

¹ School of Physics and Astronomy, University of Leeds, LS2 9JT, UK; phywjmdw@ast.leeds.ac.uk, mgh@ast.leeds.ac.uk, roud@ast.leeds.ac.uk, jcm@ast.leeds.ac.uk

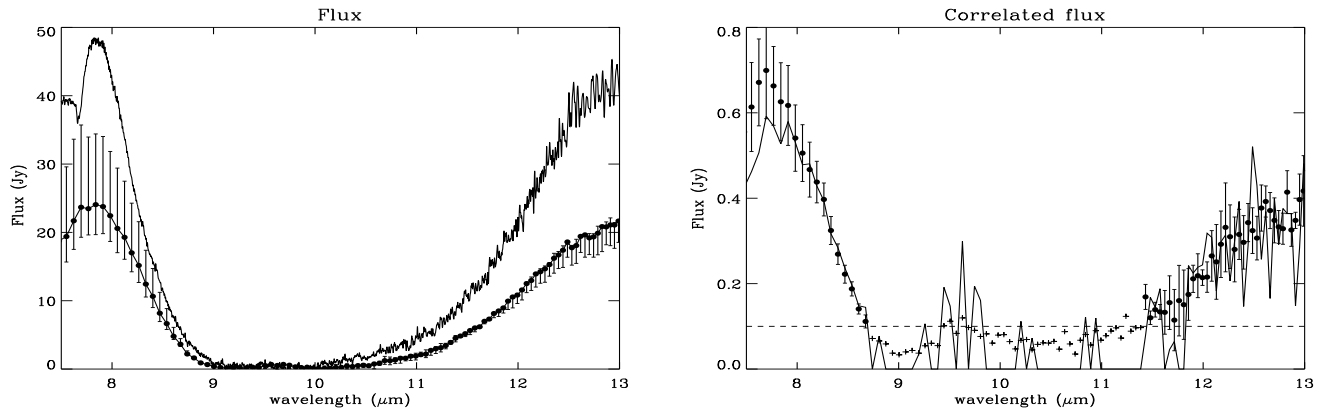


FIG. 1.— *Left:* MIDI (lower full line) and ISO flux calibrated spectra of W33A. *Right:* The correlated flux determined with EWS (dots with errorbars), and MIA (full line). Note the ragged behaviour of MIA at low flux levels. EWS errorbars correspond to the variations in visibilities as function of reduction parameters. EWS and MIA are consistent except at correlated flux levels below 0.1Jy (dashed line), these values must be considered upper limits (see Jaffe et al. 2004; Matsuura et al. 2006).

raw dataset. The two beams are interfered producing two complementary interferometric channels that have a phase difference of π radians. The dispersed fringes are modulated according to an introduced optical path delay (OPD). Interferograms are recorded for a range in OPDs, a few millimetre around optical path length equalization, called a fringe scan. For both W33A and HD 169916 a total of 8000 interferograms, corresponding to 200 scans were recorded. Subtracting the two interferometric beams eliminates the background and enhances the fringe signal. The coherent flux was extracted using two different MIDI software reduction packages: EWS (Jaffe 2004) and MIA (Köhler et al. 2005). MIA estimates the amplitudes in the power spectra of the fringe signal Fourier transform (incoherent estimation). The amplitudes are proportional to the correlated flux. EWS on the other hand aims at adding the fringes to maximize the signal to noise (coherent estimation). This method corrects first the fringe spectra for their corrupted phase caused by atmospheric and instrumental effects. EWS uses the fringe scan as phase reference to estimate the group delay due to the atmosphere. The observations show that the atmospheric group delay varied within a range of $50\mu\text{m}$ over 100s, indicating relatively good atmospheric circumstances during the night. The Fourier transform of the group delay function reveals the typical sawtooth phase change due to the introduced OPD, indicating that fringes have been measured. Removing the atmospheric and the (known) instrumental group delays constitutes a linear correction to the dispersed fringe signal, and straightens the dispersed fringe spectra, i.e. the phase is independent of wavelength. Next, the phase offset due to varying water refraction index between the time of recording of the fringe spectra has to be accounted for. In principle all spectra can then be added to a final fringe spectrum. Final visibilities are obtained by taking two spectra of the source (one with each telescope) immediately after the interferometric measurement. The accuracy of the final visibility spectrum is limited by the sky brightness variation between the interferometric and flux measurement, and can amount to 10-15%.

The flux spectra are corrected for sky contribution using a median sky subtraction. Spectra are extracted by summing the counts within 3σ of the mean position, determined from a Gaussian fit to each column along the

wavelength axis. This procedure results in a W33A spectrum with an $S/N \sim 100$ and $S/N \sim 300$ for the standard star. Four spectra are recorded, 2 for each telescope beam and combined via a geometric mean. This quantity is also what is obtained for the correlated flux after beam combination and thus ensures consistency when deriving visibilities. The absolute flux calibration is done using HD 169916, which has an average flux density of 30Jy between $8\mu\text{m}$ and $13\mu\text{m}$ (Cohen et al. 1999). The difference in airmass between the observation of the flux calibrator and W33A is 0.05 leading to a negligible correction on the final fluxes. Errorbars on the spectrum in Fig.1 indicate the systematic difference in flux levels between the two telescopes beams. Absolute flux calibration is uncertain upto at least 35% due to difference in flux level of HD 169916 in each telescope beam.

3. RESULTS

Fig. 1 presents the MIDI flux spectrum and correlated flux spectrum from EWS and MIA. The flux spectrum is compared to the ISO-SWS spectrum, taken from the ISO Data Archive maintained by ESA. Both spectra are dominated by a very strong silicate feature, that contains solid-state ammonia and methanol absorption features, at 9 and $9.7\mu\text{m}$ respectively (see Gibb et al. 2000). At the central wavelength of the feature no flux was recorded, and the actual depth is unknown. The MIDI and ISO spectra portray a similar overall shape but the MIDI spectrum has a flux level that is about a factor 2 less. In addition to the uncertainties due to flux calibration, we ascribe this difference to the much larger ISO beam ($80''$) in comparison to MIDI ($2''$).

The corresponding visibility spectrum is obtained by dividing the correlated flux by the flux spectrum and is presented in left panel of Fig. 2. Visibilities are not plotted when corresponding to correlated fluxes smaller than 0.1Jy, a value below which the measurements become unreliable (Jaffe et al. 2004, Matsuura et al. 2006). The visibility spectrum shows that the silicate wings are not strongly affected by the decrease in flux but instead follow the declining trend of the continuum visibilities. If we would represent the emission by a Gaussian emitting distribution then the FWHM size increases from 30 mas at $8\mu\text{m}$ to 60 mas at $13\mu\text{m}$.

4. RADIATIVE TRANSFER MODELLING

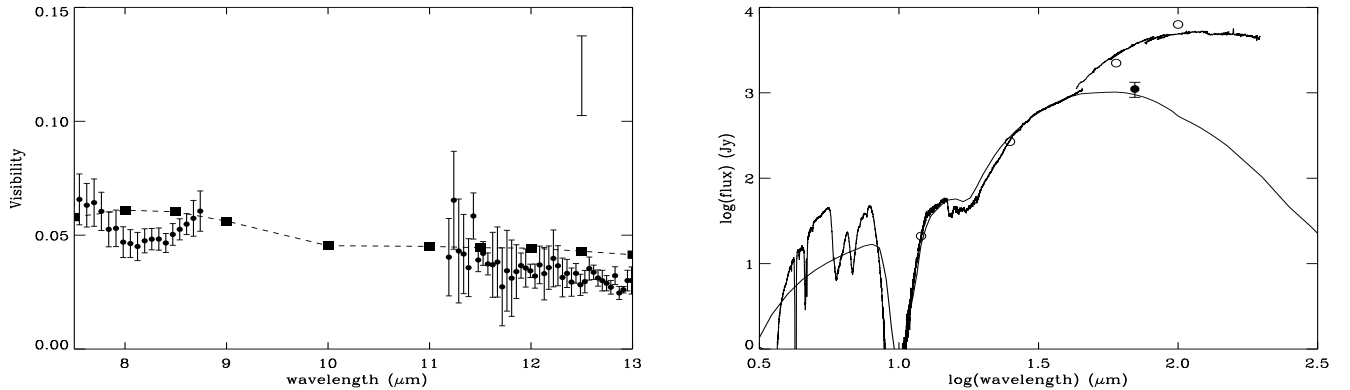


FIG. 2.— DUSTY model fits to visibilities and SED. Model is described by a $r^{-0.5}$ density law, and $A_V = 100$, star parameters are $L = 4 \cdot 10^4 L_\odot$, $T_{\text{eff}} = 10\,000\text{K}$, and a distance of 3800 pc. *Left*: Calibrated MIDI visibilities of W33A (dots with errorbars). The level of systematic uncertainty is indicated by the bar in the right top corner. Black squares connected by the dashed line correspond to the best-fit model. *Right*: SED of W33A traced by ISO-SWS and LWS spectra and IRAS points (open circles). Full line is the model fit. IRAS/ISO large beam effect at the longer wavelength is illustrated by the improved photometry using MIPS GAL images (filled circle).

Previous model fits of MYSO SEDs have indicated that simple spherical radiative transfer models with roughly constant densities best fit the near-IR and far-IR data (Churchwell et al. 1990; Gürtler et al. 1991). However, evidence exists that the outer envelopes (10,000 AU scales) have steeper density profiles (Hoare et al. 1990; van der Tak et al. 2000). We explore here whether the visibilities produced by material on 100 AU scales (a scale previously unexplored), and the SED can be simultaneously matched by simple 1D spherically symmetric dust models. Arguably, such models are inadequate for MYSOs which are likely to consist of circumstellar disks, bipolar cavities, etc. Despite this, we explore whether the basic levels and trends of the dispersed visibilities can be matched by a single unresolved star deeply embedded in a dusty envelope before introducing more free parameters.

For this purpose, we employ DUSTY, a code that solves the scaled 1D dust radiative transfer problem (see Ivezić & Elitzur 1997). We used a spherically symmetric dust distribution illuminated by a central, unresolved star. The only non-scaled parameter entering the code is the dust sublimation temperature. Gas emission is not taken into account by DUSTY. Solutions are independent of the central source luminosity, and the SED and visibilities can be scaled accordingly. The luminosity is the prime stellar parameter that sets the inner dust sublimation radius and thus the size scale; an increase causes the size of the emitting region to be larger, as $r_{\text{sub}} \propto \sqrt{L}$. The canonical parameters for W33A are $L = 1 \cdot 10^5 L_\odot$, 3.8 kpc (Faúndez et al. 2004) and we initially chose $T_{\text{eff}} = 25000\text{K}$ typical for $15 M_\odot$ star. These values make the underlying star larger than a main sequence B1 star, consistent with the idea that a star undergoing accretion at a high rate is swollen (e.g. Behrend & Maeder 2001). We tuned the model output to the observations by varying DUSTY’s input parameters, *viz.* radial density distribution, dust properties, and source T_{eff} . The challenge is to construct a single model that fits the observed visibilities, silicate wings, and mid-IR SED up to $100\mu\text{m}$. We restrict the SED fitting to this wavelength interval as it is well-known that 1D models have particular difficulty in reproducing the short wavelength region because of the sensitivity to the viewing

angle (cf. Yorke & Sonnhalter 2002).

We adopt a dust sublimation temperature of 1500 K and an MRN-DL dust mixture (Mathis et al. 1977; Draine & Lee 1984) with a typical interstellar graphitic-silicate composition. The outer bound of the model is set at 1000 times the dust sublimation radius, where the temperature corresponds to the presumed ambient temperature of the ISM, between 10 and 25 K. The precise value for the outer radius does not affect our conclusions here.

Previous studies have shown that W33A is best described by an A_V between 100 and 200 (Capps et al. 1978; Gürtler et al. 1991). A first result is that the MIDI visibilities cannot be reproduced for any density distributions with power exponents between -2.0 and 0.0 for A_V between 100 and 200 and $L = 1 \cdot 10^5 L_\odot$. The model visibilities at $10\mu\text{m}$ are too small by an order of magnitude. Decreasing A_V is not a solution for normal dust, because of W33A’s exceptionally strong silicate absorption feature. Average model sizes at $10\mu\text{m}$ of $\sim 200\text{AU}$ are reached only if the luminosity is reduced to about a third. Such a reduction is justified when we consider $70\mu\text{m}$ MIPS GAL data that we have obtained from the Spitzer archive. These data are taken at a vastly superior resolution compared to both IRAS and ISO and reveal the presence of at least three point sources and strong diffuse emission within the IRAS beam. For W33A, we measure a $70\mu\text{m}$ flux of $1.1 \cdot 10^3 \text{Jy}$ (20% uncertainty), as shown in Fig.2. This indicates that the true luminosity is significantly less than deduced from IRAS data.

Even with the luminosity reduced to $4 \cdot 10^4 L_\odot$, thermally supported cores with r^{-2} dependency (Larson 1969) are incompatible with the observed trend of decreasing visibilities with wavelength and the SED. Incompatible models are also found if we adopt a constant infall velocity type distribution with $r^{-1.5}$ (Shu 1977). Reasonable fits to the SED that produce sizes comparable to the MIDI visibilities are found for $r^{-1.0}$ logotropic distributions (e.g. McLaughlin & Pudritz 1996), but again they do not reproduce the observed decreasing visibility trend with wavelength. DUSTY produces smaller sizes, and thus larger visibilities, for longer wavelengths. This affects especially the red wing of the silicate feature, due to the diminishing opacity further out

in the silicate wing. This mismatch in visibilities is however removed if we reduce the slope to a much shallower density distribution with a $r^{-0.5}$ law or a constant density law. These distributions fit the short wavelength region of the SED increasingly worse because of the loss of warm dust. These shallower density distributions also require the luminosity of the central object to be fainter than sB9observed. We thus find that for standard ISM dust, the SED and the sizes at scales of 100 AU limit the dust to follow distributions between $r^{-1.0}$ or $r^{-0.5}$ powerlaws. The required optical depths are relatively high, yet the best models do not fit the SED particularly well.

Different dust compositions influence both the magnitude and shape of the visibility spectrum. We now explore dust made of cold and warm silicates by Ossenkopf et al. (1992) and amorphous carbon. Ossenkopf silicates have the strong advantage of a larger optical depth in the silicate feature than the DL grains. This property is advantageous in case of W33A, because it allows models with relatively moderate A_V to produce deep silicate absorption. Models with moderate extinction fit the shorter wavelength fluxes better. We find that the typical ISM ratio of 0.88 between graphite and silicates does not produce enough silicate absorption to fit W33A's strong absorption feature. A better correspondence is reached if this ratio is reduced to 0.50 (see also Churchwell et al. 1990). The warm Ossenkopf silicates bring the extra advantage of somewhat reducing the sublimation radius. Although the reduction in A_V , and a better correspondence to the silicate feature depth produces reasonable correspondence between the shallow density models with the observation, models that fit the data better are found by lowering the T_{eff} of the star. The change of this parameter produces a decrease of the size of the inner dust boundary, because of the lower dust opacity with temperature. We finally arrive at a simultaneous fit (Fig. 2) to the red silicate wing, SED peak and visibilities for a central object with a relatively low T_{eff} of 10^4 K (corresponding to a B9 supergiant, again consistent with the notion that an accreting star may be swollen) and a $r^{-0.5}$ density law (Fig. 2). The dust sublimation radius for $T_d = 1500$ K is found at 7 mas (26.5 AU).

In summary, fitting 1D DUSTY models to the visi-

bilities and SED of W33A has shown that for nominal stellar parameters, size scales of the emission region are too large and produce the wrong trend with wavelength. Shallow radial density distributions produce this trend of size with wavelength and in order to fit the depth of the silicate feature as well, dust models with warm Ossenkopf silicates with an increased silicate over graphite ratio reproduce the observation best, provided the luminosity and T_{eff} of the central object are reduced.

5. CONCLUSIONS

We presented mid-IR high-resolution dispersed interferometric observations of the forming massive star W33A. The visibility spectrum indicates an equivalent Gaussian FWHM of the emitting region of ~ 120 AU, at $8\mu\text{m}$, increasing to ~ 240 AU, at $13\mu\text{m}$. We interpreted the interferometric data with simple spherically symmetric DUSTY models representative of a (unresolved) star embedded in a dusty envelope, aiming for a simultaneous fit to the SED, silicate profile and visibility spectrum. For any radial dust distribution we found that the canonical value of W33A's luminosity is not compatible with the visibilities. This is supported by MIPS GAL data. We found that even for a reduced luminosity, the model produces too large emitting regions causing the visibilities and SED to be mutually incompatible. Changing the dust composition improves the situation for an increased graphite to silicate ratio and using warm silicate optical constants from Ossenkopf et al. (1992). We resorted to a substantial lowering of the T_{eff} in order to obtain a satisfactory match between observables and models. Further coverage of the uv-plane will be very rewarding, constraining more appropriate, higher dimensionality models, which will eventually lead in a proper description of the circumstellar environment of an accreting massive star. A full 2D axi-symmetric treatment of this and other MIDI data will be the subject of a future paper.

It is a pleasure to thank Olivier Chesneau and Rainer Köhler for discussion on the MIDI data reduction.

REFERENCES

- Behrend, R., & Maeder, A. 2001, *A&A*, 373, 190
 Beltrán, M. T., et al. 2006, *Nature*, 443, 427
 Beuther, H., et al. 2007, in *Protostars and Planets V*, ed. B. Reipurth, D. Jewitt, & K. Keil, 165
 Bunn, J. C., Hoare, M. G., & Drew, J. E. 1995, *MNRAS*, 272, 346
 Capps, R. W., Gillett, F. C., & Knacke, R. F. 1978, *ApJ*, 226, 863
 Chesneau, O., et al. 2005, *A&A*, 435, 563
 Cohen, M. et al 1999, *AJ*, 117, 1864
 Churchwell, E., Wolfire, M., & Wood, D. 1990, *ApJ*, 354, 247
 De Buizer, J. M. 2006, *ApJ*, 642, L57
 Draine, B. T., & Lee, H. M. 1984, *ApJ*, 285, 89
 Faúndez, et al. 2004, *A&A*, 426, 97
 Gibb, E. L., et al. 2000, *ApJ*, 536, 347
 Guertler, J., et al. 1991, *ApJ*, 642, L57
 Hoare, M. G. 1990, *MNRAS*, 244, 193
 Hoare, M. G. 2002, in *ASPC 267*, ed. P. Crowther, 137
 Hoare, M. G., et al. 2007, in *Protostars and Planets V*, ed. B. Reipurth, D. Jewitt, & K. Keil, 181
 Ivezić, Z., & Elitzur, M. 1997, *MNRAS*, 287, 799
 Jaffe, W. J. 2004, in *SPIE 5491*, ed. W. A. Traub, 715
 Köhler, R. 2005, *Astronomische Nachrichten*, 326, 563
 Kraemer, et al. 2001, *ApJ*, 561, 282
 Larson, R. B. 1969, *MNRAS*, 145, 271
 Leinert, C., et al. 2003, *The Messenger*, 112, 13
 Leinert, C., et al. 2004, *A&A*, 423, 537
 Mathis, J. S., Rumpl, W., & Nordsieck, K. H. 1977, *ApJ*, 217, 425
 Matsuura, M., et al. 2006, *ApJ*, 646, L123
 McLaughlin, D. E., & Pudritz, R. E. 1996, *ApJ*, 469, 194
 Mottram, J. C., et al. 2007, *ArXiv 0709*, 2040
 Nather, R. 1972, PhD thesis, University of Cape Town
 Ossenkopf, V., Henning, T., & Mathis, J. S. 1992, *A&A*, 261, 567
 Pasinetti Fracassini, et al. 2001, *A&A*, 367, 521
 Patel, N. A., et al. 2005, *Nature*, 437, 109
 Przygodda, F., et al. 2003, *Ap&SS*, 286, 85
 Rengarajan, T. N., & Ho, P. T. P. 1996, *ApJ*, 465, 363
 Shu, F. H. 1977, *ApJ*, 214, 488
 Torrelles, J. M., et al. 2007, *ApJ*, 666, L37
 van der Tak, F. F. S., & Menten, K. M. 2005, *A&A*, 437, 947
 van der Tak, F. F. S., et al. 2000, *ApJ*, 537, 283
 Yorke, H. W., & Sonnhalter, C. 2002, *ApJ*, 569, 846